

Doubly charmed tetraquark T_{cc}^+ from Lattice QCD near Physical Point

Yan Lyu,^{1,2,*} Sinya Aoki,^{3,2,†} Takumi Doi,^{2,‡} Tetsuo Hatsuda,^{2,§} Yoichi Ikeda,^{4,¶} and Jie Meng^{1,5,**}

¹State Key Laboratory of Nuclear Physics and Technology,
School of Physics, Peking University, Beijing 100871, China

²Interdisciplinary Theoretical and Mathematical Sciences Program (iTHEMS), RIKEN, Wako 351-0198, Japan

³Center for Gravitational Physics, Yukawa Institute for Theoretical Physics, Kyoto University, Kyoto 606-8502, Japan

⁴Center for Infectious Disease Education and Research, Osaka University, Suita 565-0871, Japan

⁵Yukawa Institute for Theoretical Physics, Kyoto University, Kyoto 606-8502, Japan

(Dated: February 21, 2023)

The doubly charmed tetraquark T_{cc}^+ recently discovered by the LHCb collaboration is studied on the basis of $(2+1)$ -flavor lattice QCD simulations of D^*D system with nearly physical pion mass $m_\pi = 146$ MeV. The interaction of D^*D in the isoscalar and S -wave channel, derived from the hadronic spacetime correlation by the HAL QCD method, is attractive for all distances and leads to a near-threshold virtual state with a pole position $E_{\text{pole}} \simeq -45$ keV and a large scattering length $1/a_0 \simeq 0.05$ fm⁻¹. The virtual state is shown to evolve into a loosely bound state as m_π decreases to its physical value based on an extrapolation of the interaction to $m_\pi = 135$ MeV: The extrapolated result is found to give a semi-quantitative description of the LHCb data on the $D^0D^0\pi^+$ mass spectrum.

Introduction.— The quest of exotic hadrons with multi-quark configuration beyond the conventional constituent quark model has been one of central subjects in the study of nonperturbative QCD for decades [1–6]. Although dozens of candidates of exotic hadrons were reported [7, 8], a doubly charmed tetraquark T_{cc}^+ was discovered only recently by the LHCb collaboration [9]: A pronounced narrow peak appears in the $D^0D^0\pi^+$ mass spectrum just around 360 keV below $D^{*+}D^0$ threshold, and its isospin I , spin J and parity P are found to be consistent with $(I, J^P) = (0, 1^+)$ [10].

Although early theoretical predictions on the mass of T_{cc}^+ were scattered in the range of ± 300 MeV with respect to the $D^{*+}D^0$ threshold, the constraint from the LHCb data starts to lead a consistent description on the basic properties of T_{cc}^+ in recent phenomenological models (see Refs. [11–22] and references therein). Nevertheless, a solid theoretical validation on the existence of T_{cc}^+ needs to be given from first-principles lattice QCD simulations. So far, the lattice QCD studies on the doubly charmed tetraquark in terms of the D^*D scattering length [23–25] and the finite-volume D^*D energy [26, 27] have been limited in the region of large pion masses ($m_\pi \geq 280$ MeV) and small lattice sizes ($L \leq 2.9$ fm).

Under the above circumstances, the purpose of this Letter is twofold. Our first purpose is to report a realistic investigation of the D^*D scattering in the $I = 0$ and S -wave channel from lattice QCD simulations with nearly physical pion mass $m_\pi = 146$ MeV and a large lattice size $L = 8.1$ fm. We employ the HAL QCD method [28–30], which can convert the hadronic spacetime correlation to the physical observables through an effective interaction potential. Shown in Fig. 1 is a summary of the previous lattice QCD calculations of the inverse scattering length of D^*D as a function of m_π^2 . The recent result of LHCb

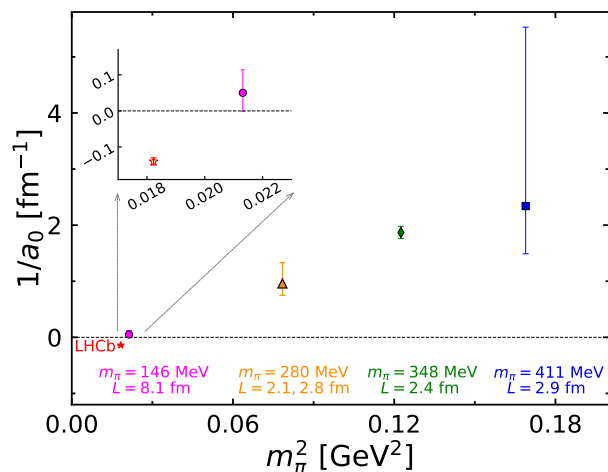


FIG. 1. The inverse of scattering length $1/a_0$ for the D^*D scattering in the $I = 0$ and S -wave channel obtained from lattice QCD simulations by Refs. [23] (blue square), [24] (green diamond), and [25] (yellow triangle). The result of the present paper and the real part of the experimental value by the LHCb collaboration [10] are shown by the magenta circle and the red star, respectively.

and the result of the present paper at $m_\pi = 146$ MeV to be described below are also shown. Fig. 1 indicates a clear trend that the lattice data approach to the experimental data as the pion mass decreases toward the physical point. While it is of primary importance to examine the D^*D scattering parameters and the pole position of T_{cc}^+ , a direct comparison between theoretical and experimental mass spectrum is also valuable to unveil the properties of near-threshold tetraquark. Therefore, our second purpose is to calculate $D^0D^0\pi^+$ mass spectrum using our result for a direct comparison with the

LHCb data. The HAL QCD method is best suited for such comprehensive analysis, since it provides the D^*D scattering T -matrix from the interaction potential and allows us to study how the spectrum changes toward the physical point.

HAL QCD method.— The starting point for deriving D^*D interaction in the HAL QCD method is the normalized spacetime correlation [28–30],

$$\begin{aligned} R(\mathbf{r}, t) &= \sum_{\mathbf{x}} \langle 0 | D^*(\mathbf{x} + \mathbf{r}, t) D(\mathbf{x}, t) \bar{\mathcal{J}}(0) | 0 \rangle / e^{-(m_{D^*} + m_D)t} \\ &= \sum_n A_n \psi_n(\mathbf{r}) e^{-(\Delta E_n)t} + O(e^{-(\Delta E^*)t}), \end{aligned} \quad (1)$$

where the energy shift is defined as $\Delta E_n = E_n - (m_{D^*} + m_D)$ with $E_n = \sqrt{m_{D^*}^2 + \mathbf{k}_n^2} + \sqrt{m_D^2 + \mathbf{k}_n^2}$, and \mathbf{k}_n being relative momentum in the center of mass frame. The wall-type source operator \mathcal{J} at $t = 0$, which has a large coupling with the low-energy scattering states, is adopted together with Coulomb gauge fixing. The coupling strength to the scattering state is denoted by $A_n = \langle E_n | \bar{\mathcal{J}}(0) | 0 \rangle$. For the sink, we use local operators of the form $\bar{q}(x)\Gamma c(x)$ with $\Gamma = \gamma_i$ for D^* and $\Gamma = \gamma_5$ for D , where $q(x)$ denotes either $u(x)$ or $d(x)$. The equal-time Nambu-Bethe-Salpeter (NBS) wave function for each elastic scattering state is defined as $\psi_n(\mathbf{r})$. Contributions from inelastic states are exponentially suppressed as $O(e^{-(\Delta E^*)t})$ with inelastic threshold $\Delta E^* \sim m_\pi$ for two-body scatterings. The S -wave projection of $R(\mathbf{r}, t)$ on the lattice is carried out by the Misner's method [31]. We find the non- S -wave component of $R(\mathbf{r}, t)$ is highly suppressed to only $O(0.1 \sim 0.01)\%$, similar with the observations in Refs. [18, 25].

The correlation function $R(\mathbf{r}, t)$ is known to satisfy the partial differential equation [29, 32],

$$\begin{aligned} \left[\frac{1 + 3\delta^2}{8\mu} \partial_t^2 - \partial_t - H_0 + O(\delta^2 \partial_t^3) \right] R(\mathbf{r}, t) \\ = \int d\mathbf{r}' U(\mathbf{r}, \mathbf{r}') R(\mathbf{r}', t). \end{aligned} \quad (2)$$

where $H_0 = \frac{-\nabla^2}{2\mu}$, $\mu = \frac{m_{D^*} m_D}{m_{D^*} + m_D}$, $\delta = \frac{m_{D^*} - m_D}{m_{D^*} + m_D}$. The integral kernel $U(\mathbf{r}, \mathbf{r}')$ is defined through $[\mathbf{k}_n^2 / (2\mu) - H_0] \psi_n(\mathbf{r}) = \int d\mathbf{r}' U(\mathbf{r}, \mathbf{r}') \psi_n(\mathbf{r}')$. The $O(\delta^2 \partial_t^3)$ term is found to be consistent with zero within statistical error and is neglected in our analysis. The derivative expansion $U(\mathbf{r}, \mathbf{r}') = \sum_n V_n(\mathbf{r}) \nabla^n \delta(\mathbf{r} - \mathbf{r}')$ at the leading order gives an effective local potential,

$$V(r) = R^{-1}(\mathbf{r}, t) \left[\frac{1 + 3\delta^2}{8\mu} \partial_t^2 - \partial_t - H_0 \right] R(\mathbf{r}, t), \quad (3)$$

which has been shown to be a good approximation at low energies. The truncation error from higher-order terms can be estimated through the t -dependence of $V(r)$ [29, 33, 34]. Once the potential is obtained, it can be used to calculate physical quantities such as the scattering amplitude and the scattering phase shift by solving

the stationary Schrödinger equation, $[H_0 + V(r)]\psi(\mathbf{r}) = E\psi(\mathbf{r})$ in the infinite spatial volume.

Lattice setup.— The $(2+1)$ -flavor gauge configurations are generated on the 96^4 lattice with the Iwasaki gauge action and the nonperturbatively $O(a)$ -improved Wilson quark action at nearly physical point ($m_\pi = 146.4$ MeV) [35]. The lattice spacing is $a = 0.0846$ fm, corresponding to lattice size $L = 8.1$ fm. For the charm quark, the relativistic heavy quark (RHQ) action is employed in order to remove the cutoff errors associated with the charm quark mass up to next-to-next-to-leading order [36]. The charm quark mass is set to be very close to its physical value, which leads to a spin-averaged $1S$ charmonium mass $M_{\text{av}} \equiv (m_{\eta_c} + 3m_{J/\psi})/4 = 3096.6$ MeV, 0.9% larger than the physical value [37]. By comparing results from another set of RHQ parameters corresponding to $M_{\text{av}} = 3051.4$ MeV, 0.6% smaller than the physical value, we confirm that effect from slightly unphysical charm quark is small compared with current statistical uncertainties.

We use 200 gauge configurations, and 640 measurements (= 4 directions \times 80 source positions \times 2 forward/backward propagations) [38] are performed for each configuration to increase the statistics. The jackknife method is used to estimate the statistical error with a bin size of 20 configurations throughout this Letter; comparison with a bin size of 40 configurations shows that the bin size dependence is small. The quark propagators are calculated by the domain-decomposed solver [39] and the Bridge++ code [40] with the periodic boundary condition for all directions, and the unified contraction algorithm is used to obtain the hadronic correlation functions [41]. The D^* and D masses from the single-state fit in the temporal region $t/a = 20 - 30$ are $m_{D^*} = 2018.1(6)$ MeV and $m_D = 1878.2(3)$ MeV with statistical error shown in the parenthesis. These numbers are 0.5% heavier than the physical values. With our slightly heavy pion mass, m_{D^*} becomes smaller than the $D\pi$ threshold, so that D^* is stable against strong decay. Other systematic errors are expected to be small: (i) The finite cutoff effect amounts to $O((a\Lambda_{\text{QCD}})^2, \alpha_s^2 a \Lambda_{\text{QCD}}) \simeq O(1)\%$ thanks to $O(a)$ improvement for the light quarks and RHQ action for the charm quark, (ii) the finite volume effect is expected to be as small as $\exp(-m_h(L/2)) \simeq 0.3\%$ (where $m_h = 2m_\pi$ as described below) thanks to the large volume, and (iii) the quenched charm quark effect is highly suppressed by the heavy charm quark mass.

Interaction potential.— We show in Fig. 2 the D^*D potential $V(r)$ in the $I = 0$ and S -wave channel defined in Eq. (3) for $t/a = 21, 22$, and 23 , corresponding to $t \simeq 1.9$ fm. This temporal region is chosen to suppress inelastic states contamination at smaller t and simultaneously to avoid large statistical errors at larger t . A variation of the potentials for different t/a , smaller than the statistical error, is taken into account as a source of the systematic error. It indicates that the systematic er-

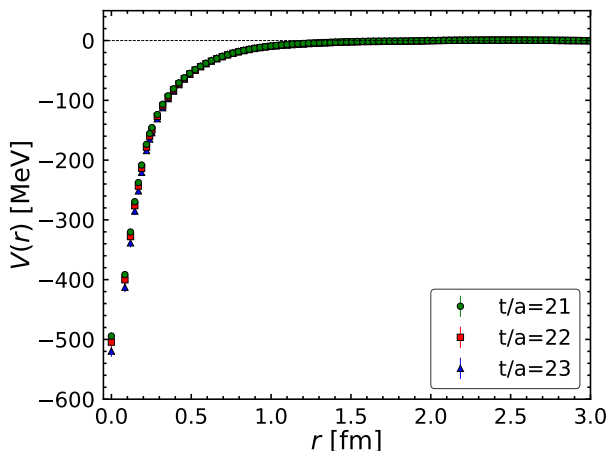


FIG. 2. The D^*D potential $V(r)$ in the $I = 0$ and S -wave channel at Euclidean time $t/a = 21$ (green circles), 22 (red squares), and 23 (blue triangles).

rors from higher-order terms of the derivative expansion and from the inelastic states are small.

For later convenience, we perform an uncorrelated fit for the potential in Fig. 2 by a phenomenological three-range Gaussian form, $V_{\text{fit}}^A(r) = \sum_{i=1,2,3} a_i e^{-(r/b_i)^2}$.

Fitting parameters with $t/a = 22$ are $(a_1, a_2, a_3) = (-306(5), -128(7), -28(10))$ in MeV and $(b_1, b_2, b_3) = (0.17(1), 0.44(3), 0.95(14))$ in fm with an accuracy of $\chi^2/\text{d.o.f.} \simeq 0.5$.

The D^*D potential in the $(I, J^P) = (0, 1^+)$ channel shown in Fig. 2 is attractive for all distances. This is consistent with the result previously found for heavy pion masses by using the HAL QCD method [23]; The short-range attraction was suggested to be related to the attractive (anti)diquark configuration $(\bar{u}\bar{d})_{\mathbf{3}_c, I=J=0} - (cc)_{\mathbf{3}_c, J=1}$, coupled to the asymptotic D^*D state [42–44] (for an interpretation based on string model, see Ref. [45]). Similar short-range attraction was also found for the B^*B system in the $(I, J^P) = (0, 1^+)$ channel [46, 47]. The long-range part of the attraction for $r > 1$ fm would have contributions from the one-pion exchange between D^* and D of the form $\sim e^{-m_\pi r}/r$ with either $m = m_\pi$ [48] or $m = \sqrt{(m_{D^*} - m_D)^2 - m_\pi^2}$ [49], and from the two-pion exchange of the form $\sim (e^{-m_\pi r}/r)^2$ [38].

To study different possibilities for the long-range part, we introduce the following fit function with the Gaussian-type form factor [38];

$$V_{\text{fit}}^B(r; m_\pi) = \sum_{i=1,2} a_i e^{-(r/b_i)^2} + a_3 (1 - e^{-(r/b_3)^2}) n V_\pi^n(r)$$

with $V_\pi(r) = e^{-m_\pi r}/r$. We find that $n = 2$ and $m_\pi = 146.4$ MeV provide a best fit with the parameter set, $(a_1, a_2) = (-284(36), -201(60))$ in MeV, $a_3 = -45(12)$ MeV \cdot fm², and $(b_1, b_2, b_3) =$

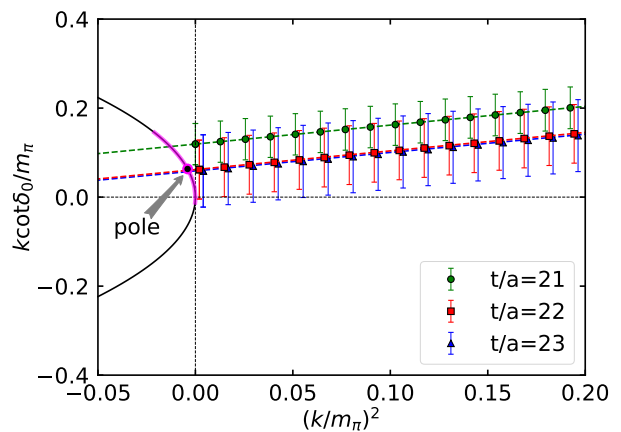


FIG. 3. The $k \cot \delta_0/m_\pi$ for D^*D scattering in the $I = 0$ and S -wave channel as a function of $(k/m_\pi)^2$. The black solid line represents $\pm\sqrt{-(k/m_\pi)^2}$, and its intersection with $k \cot \delta_0/m_\pi$ denotes the pole of the scattering amplitude. The pole position is shown by the black point with magenta line showing corresponding statistical and systematic errors combined. For visibility, data are a little shifted horizontally.

$(0.15(2), 0.32(12), 0.49(24))$ in fm. Also, we find that $n = 1$ and $m_\pi = 146.4$ MeV nor $n = 1$ and $m_\pi \rightarrow \sqrt{(m_{D^*} - m_D)^2 - m_\pi^2}$ cannot reproduce the long-range part of the potential. In Fig. S1 of the the Suppl. Material [50], we show the spatial effective energy defined as $E_{\text{eff}}(r) = -\frac{\ln[V(r)r^2/a_3]}{r}$ with the lattice data for $V(r)$ and a_3 as inputs: $E_{\text{eff}}(r)$ shows a plateau at $2m_\pi = 292.8$ MeV for $1 < r < 2$ fm, which indicates that the long-range part is consistent with two-pion exchange. It is an open question why the theoretically possible one-pion exchange contribution cannot be seen in the lattice data.

Scattering parameters and pole position.— Using the potential fitted to our lattice data, we calculate the S -wave scattering phase shifts δ_0 by solving the Schrödinger equation with $m_{D^*,D}$ measured on the lattice. Fig. 3 shows the $k \cot \delta_0/m_\pi$ as a function of $(k/m_\pi)^2$ with k being a relative momentum. The scattering length a_0 and the effective range r_{eff} are obtained by an effective-

TABLE I. Results for the inverse of scattering length $1/a_0$, the effective range r_{eff} , the pole position κ_{pole} , and E_{pole} . Numbers in the 2nd column with statistical error in the first parenthesis and systematic error in the second parenthesis are obtained by using $V_{\text{fit}}^{A,B}(r)$ with $t/a = 21 - 23$ at $m_\pi = 146.4$ MeV, while the 3rd column shows corresponding estimated values with statistical errors using an extrapolation of $V_{\text{fit}}^B(r)$ with $t/a = 22$ to $m_\pi = 135.0$ MeV.

m_π [MeV]	146.4	135.0
$1/a_0$ [fm ⁻¹]	0.05(5) $\left(\begin{smallmatrix} +4 \\ -1 \end{smallmatrix}\right)$	-0.02(4)
r_{eff} [fm]	1.14(6) $\left(\begin{smallmatrix} +1 \\ -9 \end{smallmatrix}\right)$	1.14(8)
κ_{pole} [MeV]	-9(9) $\left(\begin{smallmatrix} +1 \\ -8 \end{smallmatrix}\right)$	+3(8)
E_{pole} [keV]	-45(77) $\left(\begin{smallmatrix} +02 \\ -99 \end{smallmatrix}\right)$	-10(37)

range expansion (with the sign convention of high-energy physics) as

$$k \cot \delta_0 = \frac{1}{a_0} + \frac{1}{2} r_{\text{eff}} k^2 + O(k^4), \quad (5)$$

and are given in the 2nd column of TABLE I. The central values and the statistical errors in the first parentheses are obtained at $t/a = 22$ with V_{fit}^B , while the systematic errors in the second parentheses are obtained by comparing results from different $t/a = 21 - 23$ with $V_{\text{fit}}^{A,B}$.

The scattering length obtained in this way is shown by the magenta circle in Fig. 1 together with the previous results and the LHCb data. As mentioned in the Introduction, there is a clear tendency that $1/a_0$ from lattice data approaches to the unitary regime ($1/a_0 \sim 0$) as the pion mass decreases. Also, our result at $m_\pi = 146.4$ MeV produces a virtual state. This implies that a marginal modification of the interaction, e.g. by reducing the quark mass, may bring such a near-threshold virtual state to a loosely bound state. An example of virtual/bound state sensitive to the quark mass is dineutron/deuteron in nuclear physics [51–53]. A bound (virtual) state is characterized by a pole of the scattering amplitude $f(k)$ on the positive (negative) side of the imaginary axis at $k = i\kappa_{\text{pole}}$. Since $f^{-1}(k)$ is proportional to $k \cot \delta_0$, virtual and bound poles near threshold can be inferred from the intersection between $\frac{1}{a_0} + \frac{1}{2} r_{\text{eff}} k^2$ and $\pm \sqrt{-k^2}$. As shown in Fig. 3, we indeed find a near-threshold virtual state pole. The actual value of the pole position in the complex k -plane for the present pion mass is shown in the 2nd column of TABLE I, together with the energy of the pole defined by $E_{\text{pole}} = \sqrt{m_{D^*}^2 - \kappa_{\text{pole}}^2} + \sqrt{m_D^2 - \kappa_{\text{pole}}^2} - (m_{D^*} + m_D)$.

To estimate how the scattering parameters change and the pole evolves towards the physical point, we extrapolate the potential by taking $m_\pi = 135.0$ MeV (\sim the physical pion mass without the QED contribution) with the other parameters ($a_{1,2,3}, b_{1,2,3}$) of V_{fit}^B at $t/a = 22$ kept fixed. Using such a potential together with physical m_{D^{*+}, D^0} [54] we find a loosely bound state with the scattering parameters and pole positions given in the 3rd column of TABLE I. This indicates the existence of a bound T_{cc}^+ at physical point, though there is still a quantitative difference from the experimental value $E_{\text{pole}} = -360(40) \left(\begin{smallmatrix} +4 \\ -0 \end{smallmatrix} \right)$ keV reported by LHCb collaboration [10]. Since the binding energy is very sensitive not only to the quark masses but also to the isospin symmetry breaking effect, further works should be necessarily by $(1+1+1)$ -flavor or $(1+1+1+1)$ -flavor lattice QCD + QED simulations to make a precise comparison.

Here we make an alternative estimate of the scattering length at the physical point by taking the present and previous lattice data shown in Fig. 1: By using simplest fit function $1/a_0(m_\pi) = c + dm_\pi^2$, the scattering length for $m_\pi = 135.0$ MeV reads $1/a_0 = -0.01(9)$ fm $^{-1}$ (Fig. S2 in the Suppl. Material [50]). This result is consistent

with $1/a_0 = -0.02(4)$ fm $^{-1}$ obtained by V_{fit}^B extrapolated to the same pion mass, which indicates that the chiral extrapolation of the V_{fit}^B is reasonable.

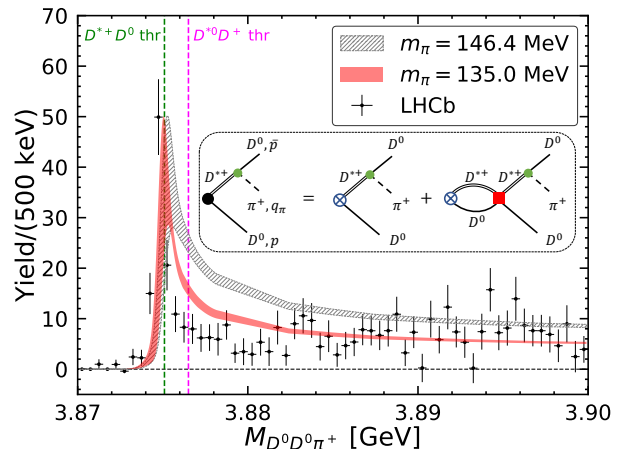


FIG. 4. The $D^0 D^0 \pi^+$ mass spectrum. Our theoretical calculation with $V_{\text{fit}}^B(r; m_\pi)$ for $m_\pi = 146.4$ MeV ($m_\pi = 135.0$ MeV) is shown by the gray (red) band. The black points are LHCb data [10]. The inset shows diagrams contributing to the $D^0 D^0 \pi^+$ mass spectrum, where the black filled circle, blue cross circle, green filled circle, and red square denote production amplitude U , constant vertex P , $D^{*+} \rightarrow D^0 \pi^+$ vertex, and scattering T matrix, respectively.

$D^0 D^0 \pi^+$ mass spectrum.— In order to make a further connection to the LHCb experimental data, let us now construct $D^0 D^0 \pi^+$ mass spectrum based on the above interaction by considering the rescattering between D^{*+} and D^0 along the line with Refs. [18, 55]. For this purpose, we first construct a production amplitude $U(M, p)$ for $D^{*+} D^0$ pair with invariant mass M and relative momentum p in the $I = 0$ and S -wave channel generated from a constant vertex P . Then the amplitude consists of a direct production process and a rescattering process and can be written as (see the inset in Fig. 4),

$$U(M, p) = P + \int \frac{d^3 \mathbf{q}}{(2\pi)^3} T(M, p, q) G(M, q) P. \quad (6)$$

Here the scattering T -matrix $T(M, p, q)$ with in-coming (out-going) momentum q (p) are obtained by solving the Lippmann-Schwinger equation with a given potential. The $D^{*+} D^0$ propagator is denoted as $G(M, q) = \left(M - m_{D^{*+}} - m_{D^0} - \frac{q^2}{2\mu} + \frac{i}{2} \Gamma_{D^{*+}} \right)^{-1}$ where $\Gamma_{D^{*+}}$ is the decay width of D^{*+} , representing the unstable nature of D^{*+} in the real world. For m_{D^{*+}, D^0} and $\Gamma_{D^{*+}}$, experimental values are taken [54]. We set $P = 1$ without loss of generality, since it can be absorbed into an overall normalization factor. Then, the $D^0 D^0 \pi^+$ mass spectrum reads

$$\frac{d\text{Br}[D^0 D^0 \pi^+]}{dM} = \mathcal{N} \int p dp \int \bar{p} d\bar{p} |U(M, p) G(M, p) q_\pi(p) + U(M, \bar{p}) G(M, \bar{p}) q_\pi(\bar{p})|^2, \quad (7)$$

where the pion momentum $q_\pi(p)$ arises from $D^{*+} \rightarrow D^0\pi^+$ vertex, and can be determined kinematically [18]. The second term of the integrand with \bar{p} comes from symmetrizing the $D^0D^0\pi^+$ amplitude due to two identical D^0 s in the final state. With \mathcal{N} being an overall normalization factor, the shape of $D^0D^0\pi^+$ mass spectrum does not depend on any free parameters in the above construction. In order to compare with the LHCb data, an energy resolution function given in Ref. [10] is convolved with Eq. (7).

Shown in Fig 4 by the gray band and the red band are our theoretical calculations for $D^0D^0\pi^+$ mass spectrum obtained by using $V_{\text{fit}}^B(r; m_\pi)$ with $m_\pi = 146.4$ MeV and $m_\pi = 135.0$ MeV, respectively. Shown together by the black points are LHCb data [10]. The obtained mass spectrum has a pronounced peak around the $D^{*+}D^0$ threshold, and the peak position shifts to the left as m_π decreases; this is consistent with the trend of evolution from a near-threshold virtual state into a loosely bound state. At the physical pion mass, the red band with a peak just on the $D^{*+}D^0$ threshold provides a better description than the gray band to LHCb data, though visible differences still exist between the red band and LHCb data, which calls for a direct calculation of the potential with the physical pion mass as well as with the isospin symmetry breaking effect as mentioned before.

Summary and discussion.— In this Letter, we present a realistic investigation on the scattering properties of the D^*D system based on the $(2+1)$ -flavor lattice QCD simulations with nearly physical pion mass $m_\pi = 146$ MeV. The attractive potential between D^* and D in the $I = 0$ and S -wave channel is extracted from hadronic spacetime correlation. The long range part of the potential is found to be dominated by the two-pion exchange at least in the range $1 < r < 2$ fm. The overall attraction is found to be strong enough to lead a near-threshold virtual state with a pole position $E_{\text{pole}} \simeq -45$ keV and a large scattering length $1/a_0 \simeq 0.05$ fm $^{-1}$. The virtual state is shown to evolve into a loosely bound state at the physical point based on an extrapolation of the potential to $m_\pi = 135$ MeV. Such an extrapolation can also provide a semi-quantitative description to the $D^0D^0\pi^+$ mass spectrum measured by the LHCb collaboration.

We are currently underway to perform physical-point simulations in $(2+1)$ -flavor QCD. It is also an important future problem to study the isospin-breaking effect by lattice QCD + QED with the $D^{*+}D^0 - D^{*0}D^+$ coupled-channel analysis.

Acknowledgments.— We thank members of the HAL QCD Collaboration for stimulating discussions. Y.L. thanks Meng-Lin Du, and Xu Feng for the helpful discussions. We thank members of the PACS Collaboration for the gauge configuration generation conducted on the K computer at RIKEN. The lattice QCD measurements have been performed on Fugaku and HOKUSAI supercomputers at RIKEN. We thank

ILDG/JLDG [56], which serves as essential infrastructure in this study. This work was partially supported by HPCI System Research Project (hp120281, hp130023, hp140209, hp150223, hp150262, hp160211, hp170230, hp170170, hp180117, hp190103, hp200130, hp210165, hp210212, hp220240, hp220066, and hp220174), the National Key R&D Program of China (Contract No. 2018YFA0404400), the National Natural Science Foundation of China (Grant Nos. 11935003, 11975031, 11875075, 12070131001, and 12141501), the JSPS (Grant Nos. JP18H05236, JP22H00129, JP19K03879, JP18H05407, and JP21K03555), “Priority Issue on Post-K computer” (Elucidation of the Fundamental Laws and Evolution of the Universe), “Program for Promoting Researches on the Supercomputer Fugaku” (Simulation for basic science: from fundamental laws of particles to creation of nuclei), and Joint Institute for Computational Fundamental Science (JICFuS).

* helvetia@pku.edu.cn

† saoki@yukawa.kyoto-u.ac.jp

‡ doi@ribf.riken.jp

§ thatsuda@riken.jp

¶ yikeda@cider.osaka-u.ac.jp

** mengj@pku.edu.cn

- [1] H.-X. Chen, W. Chen, X. Liu, and S.-L. Zhu, Phys. Rept. **639**, 1 (2016), arXiv:1601.02092 [hep-ph].
- [2] A. Esposito, A. Pilloni, and A. D. Polosa, Phys. Rept. **668**, 1 (2017), arXiv:1611.07920 [hep-ph].
- [3] R. F. Lebed, R. E. Mitchell, and E. S. Swanson, Prog. Part. Nucl. Phys. **93**, 143 (2017), arXiv:1610.04528 [hep-ph].
- [4] A. Ali, J. S. Lange, and S. Stone, Prog. Part. Nucl. Phys. **97**, 123 (2017), arXiv:1706.00610 [hep-ph].
- [5] F.-K. Guo, C. Hanhart, U.-G. Meißner, Q. Wang, Q. Zhao, and B.-S. Zou, Rev. Mod. Phys. **90**, 015004 (2018), [Erratum: Rev.Mod.Phys. 94, 029901 (2022)], arXiv:1705.00141 [hep-ph].
- [6] Y. Yamaguchi, A. Hosaka, S. Takeuchi, and M. Takizawa, J. Phys. G **47**, 053001 (2020), arXiv:1908.08790 [hep-ph].
- [7] S. L. Olsen, T. Skwarnicki, and D. Zieminska, Rev. Mod. Phys. **90**, 015003 (2018), arXiv:1708.04012 [hep-ph].
- [8] N. Brambilla, S. Eidelman, C. Hanhart, A. Nefediev, C.-P. Shen, C. E. Thomas, A. Vairo, and C.-Z. Yuan, Phys. Rept. **873**, 1 (2020), arXiv:1907.07583 [hep-ex].
- [9] R. Aaij *et al.* (LHCb), Nature Phys. **18**, 751 (2022), arXiv:2109.01038 [hep-ex].
- [10] R. Aaij *et al.* (LHCb), Nature Commun. **13**, 3351 (2022), arXiv:2109.01056 [hep-ex].
- [11] J. P. Ader, J. M. Richard, and P. Taxil, Phys. Rev. D **25**, 2370 (1982).
- [12] H. J. Lipkin, Phys. Lett. B **172**, 242 (1986).
- [13] S. Zouzou, B. Silvestre-Brac, C. Gignoux, and J. M. Richard, Z. Phys. C **30**, 457 (1986).
- [14] D. Janc and M. Rosina, Few Body Syst. **35**, 175 (2004), arXiv:hep-ph/0405208.
- [15] D. Ebert, R. N. Faustov, V. O. Galkin, and W. Lucha,

- Phys. Rev. D **76**, 114015 (2007), arXiv:0706.3853 [hep-ph].
- [16] A. Esposito, M. Papinutto, A. Pilloni, A. D. Polosa, and N. Tantalo, Phys. Rev. D **88**, 054029 (2013), arXiv:1307.2873 [hep-ph].
- [17] M. Karliner and J. L. Rosner, Phys. Rev. Lett. **119**, 202001 (2017), arXiv:1707.07666 [hep-ph].
- [18] M.-L. Du, V. Baru, X.-K. Dong, A. Filin, F.-K. Guo, C. Hanhart, A. Nefediev, J. Nieves, and Q. Wang, Phys. Rev. D **105**, 014024 (2022), arXiv:2110.13765 [hep-ph].
- [19] X.-Z. Ling, M.-Z. Liu, L.-S. Geng, E. Wang, and J.-J. Xie, Phys. Lett. B **826**, 136897 (2022), arXiv:2108.00947 [hep-ph].
- [20] Y. Kim, M. Oka, and K. Suzuki, Phys. Rev. D **105**, 074021 (2022), arXiv:2202.06520 [hep-ph].
- [21] S. S. Agaev, K. Azizi, and H. Sundu, JHEP **06**, 057 (2022), arXiv:2201.02788 [hep-ph].
- [22] H.-X. Chen, W. Chen, X. Liu, Y.-R. Liu, and S.-L. Zhu, Rept. Prog. Phys. **86**, 026201 (2023), arXiv:2204.02649 [hep-ph].
- [23] Y. Ikeda, B. Charron, S. Aoki, T. Doi, T. Hatsuda, T. Inoue, N. Ishii, K. Murano, H. Nemura, and K. Sasaki, Phys. Lett. B **729**, 85 (2014), arXiv:1311.6214 [hep-lat].
- [24] S. Chen, C. Shi, Y. Chen, M. Gong, Z. Liu, W. Sun, and R. Zhang, Phys. Lett. B **833**, 137391 (2022), arXiv:2206.06185 [hep-lat].
- [25] M. Padmanath and S. Prelovsek, Phys. Rev. Lett. **129**, 032002 (2022), arXiv:2202.10110 [hep-lat].
- [26] G. K. C. Cheung, C. E. Thomas, J. J. Dudek, and R. G. Edwards (Hadron Spectrum), JHEP **11**, 033 (2017), arXiv:1709.01417 [hep-lat].
- [27] P. Junnarkar, N. Mathur, and M. Padmanath, Phys. Rev. D **99**, 034507 (2019), arXiv:1810.12285 [hep-lat].
- [28] N. Ishii, S. Aoki, and T. Hatsuda, Phys. Rev. Lett. **99**, 022001 (2007).
- [29] N. Ishii, S. Aoki, T. Doi, T. Hatsuda, Y. Ikeda, T. Inoue, K. Murano, H. Nemura, and K. Sasaki (HAL QCD Collaboration), Physics Letters B **712**, 437 (2012).
- [30] S. Aoki and T. Doi, Frontiers in Physics **8**, 307 (2020).
- [31] T. Miyamoto, Y. Akahoshi, S. Aoki, T. Aoyama, T. Doi, S. Gongyo, and K. Sasaki, Phys. Rev. D **101**, 074514 (2020).
- [32] S. Aoki, N. Ishii, T. Doi, T. Hatsuda, Y. Ikeda, T. Inoue, K. Murano, H. Nemura, and K. Sasaki (HAL QCD), Proc. Japan Acad. B **87**, 509 (2011), arXiv:1106.2281 [hep-lat].
- [33] T. Iritani, S. Aoki, T. Doi, T. Hatsuda, Y. Ikeda, T. Inoue, N. Ishii, H. Nemura, and K. Sasaki (HAL QCD Collaboration), JHEP **03**, 007 (2019), arXiv:1812.08539 [hep-lat].
- [34] Y. Lyu, H. Tong, T. Sugiura, S. Aoki, T. Doi, T. Hatsuda, J. Meng, and T. Miyamoto, Phys. Rev. D **105**, 074512 (2022).
- [35] K.-I. Ishikawa, N. Ishizuka, Y. Kuramashi, Y. Nakamura, Y. Namekawa, Y. Taniguchi, N. Ukita, T. Yamazaki, and T. Yoshie (PACS Collaboration), Proc. Sci. **LAT-TICE2015**, 075 (2016), arXiv:1511.09222 [hep-lat].
- [36] S. Aoki, Y. Kuramashi, and S.-i. Tominaga, Prog. Theor. Phys. **109**, 383 (2003), arXiv:hep-lat/0107009.
- [37] Y. Namekawa (PACS Collaboration), Proc. Sci. **LAT-TICE2016**, 125 (2017).
- [38] Y. Lyu, T. Doi, T. Hatsuda, Y. Ikeda, J. Meng, K. Sasaki, and T. Sugiura, Phys. Rev. D **106**, 074507 (2022), arXiv:2205.10544 [hep-lat].
- [39] K.-I. Ishikawa, I. Kanamori, H. Matsufuru, I. Miyoshi, Y. Mukai, Y. Nakamura, K. Nitadori, and M. Tsuji, Comput. Phys. Commun. **282**, 108510 (2023), arXiv:2109.10687 [hep-lat].
- [40] http://bridge.kek.jp/Lattice-code/index_e.html.
- [41] T. Doi and M. G. Endres, Comput. Phys. Commun. **184**, 117 (2013), arXiv:1205.0585 [hep-lat].
- [42] A. Selem and F. Wilczek, in *Ringberg Workshop on New Trends in HERA Physics 2005* (2006) pp. 337–356, arXiv:hep-ph/0602128.
- [43] C.-R. Deng and S.-L. Zhu, Sci. Bull. **67**, 1522 (2022), arXiv:2204.11079 [hep-ph].
- [44] S. Noh, W. Park, and S. H. Lee, Phys. Rev. D **103**, 114009 (2021), arXiv:2102.09614 [hep-ph].
- [45] O. Andreev, Phys. Rev. D **105**, 086025 (2022), arXiv:2111.14418 [hep-ph].
- [46] S. Aoki and T. Aoki, in *39th International Symposium on Lattice Field Theory* (2022) arXiv:2212.00202 [hep-lat].
- [47] P. Bicudo, K. Cichy, A. Peters, and M. Wagner, Phys. Rev. D **93**, 034501 (2016), arXiv:1510.03441 [hep-lat].
- [48] S. Ohkoda, Y. Yamaguchi, S. Yasui, K. Sudoh, and A. Hosaka, Phys. Rev. D **86**, 034019 (2012), arXiv:1202.0760 [hep-ph].
- [49] N. Li, Z.-F. Sun, X. Liu, and S.-L. Zhu, Phys. Rev. D **88**, 114008 (2013), arXiv:1211.5007 [hep-ph].
- [50] Supplemental Material at [URL].
- [51] T. Inoue, S. Aoki, T. Doi, T. Hatsuda, Y. Ikeda, N. Ishii, K. Murano, H. Nemura, and K. Sasaki (HAL QCD), Nucl. Phys. A **881**, 28 (2012), arXiv:1112.5926 [hep-lat].
- [52] B. Hörz *et al.*, Phys. Rev. C **103**, 014003 (2021), arXiv:2009.11825 [hep-lat].
- [53] S. Amarasinghe, R. Baghdadi, Z. Davoudi, W. Detmold, M. Illa, A. Parreno, A. V. Pochinsky, P. E. Shanahan, and M. L. Wagman, (2021), arXiv:2108.10835 [hep-lat].
- [54] P. A. Zyla *et al.* (Particle Data Group), Progress of Theoretical and Experimental Physics **2020** (2020), 083C01.
- [55] M. Albaladejo, Phys. Lett. B **829**, 137052 (2022), arXiv:2110.02944 [hep-ph].
- [56] <http://www.lqcd.org/ildg> and <http://www.jldg.org>.

SUPPLEMENTAL MATERIAL

We present a detailed analysis of the long-range potential and a chiral extrapolation of the inverse of scattering length in this supplemental material.

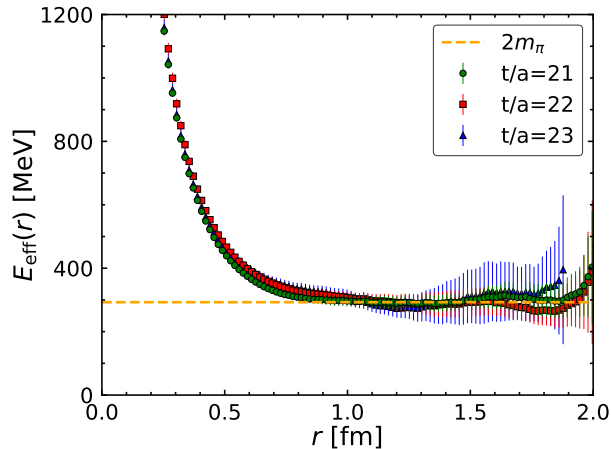


FIG. S1. The spatial effective energy $E_{\text{eff}}(r)$ as a function of separation r at Euclidean time $t/a = 21$ (green circles), 22 (red squares), and 23 (blue triangles). The orange dashed line denotes $2m_\pi$ with $m_\pi = 146.4$ MeV.

We show in Fig S1 the spatial effective energy defined as,

$$E_{\text{eff}}(r) = -\frac{\ln[V(r)r^2/a_3]}{r}, \quad (\text{S1})$$

which has a plateau at $2m_\pi = 292.8$ MeV for $r > 1.0$ fm. This numerically shows that the long-range potential is consistent with two-pion exchange form $\sim \frac{e^{-2m_\pi r}}{r^2}$.

TABLE S1. The fit parameters in Eq. S2 with 1σ uncertainty quoted in the parenthesis. The corresponding value for $1/a_0$ at $m_\pi = 135.0$ MeV is shown in the last column.

c [fm ⁻¹]	d	$\chi^2/\text{d.o.f.}$	$1/a_0$ [fm ⁻¹]
-0.33(6)	18(1) GeV ⁻² · fm ⁻¹	0.1	-0.01(9)

Shown in Fig. S2 a chiral extrapolation of lattice data for $1/a_0$ based on following fit function,

$$1/a_0(m_\pi) = c + dm_\pi^2. \quad (\text{S2})$$

Fit parameters c and d together with corresponding $1/a_0$ for $m_\pi = 135.0$ MeV are shown in Table S1. Result for $1/a_0$ from fit function agrees with the value of $1/a_0 = -0.02(4)$ fm⁻¹ from the potential extrapolated to the same pion mass, which indicates that the chiral extrapolation of the potential is reasonable.

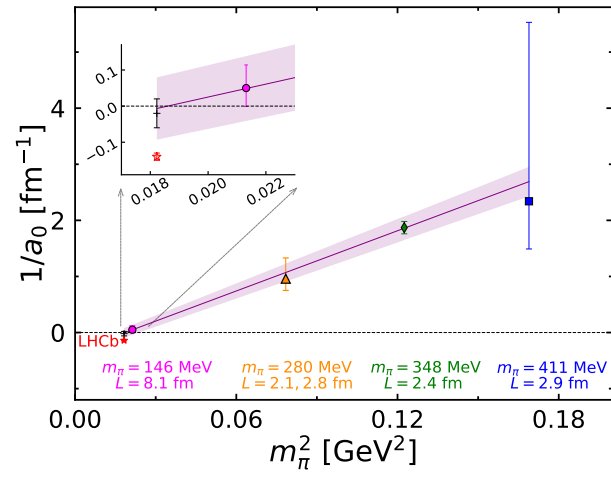


FIG. S2. The chiral extrapolation of lattice data for $1/a_0$ based on fit function in Eq. S2. The black plus symbol shows the value from the potential extrapolated to $m_\pi = 135$ MeV.